Received March 1996
Revised October 1996

Steady and unsteady computation of a two-dimensional upwash jet

Seong Ho Cho
Living System Research Laboratory, L G Electronics Inc., Seoul, Korea, and
Seung O. Park
Department of Aerospace Engineering, KAIST, Taejon, Korea

Nomenclature

B	=	jet half width	$\overline{u_i u_j}$	=	Reynolds stress
C_i	=	turbulence model coefficient	Re	=	Reynolds number
D_{ij}	=	diffusion term of the Reynolds stress	x, y	=	cartesian co-ordinate
D_w	=	height of jet nozzle	ν_t	=	turbulent eddy viscosity
G	=	production rate of turbulent kinetic energy	ε	=	dissipation of the turbulent kinetic energy
k	=	turbulent kinetic energy			
P_{ij}	=	production term of the Reynolds stress	*Subscripts*		
Φ_{ij}	=	pressure-strain correlation term of the Reynolds stress	i,j,k	=	tensor
			j	=	jet
U, V	=	mean velocity	w	=	wall
u, v	=	fluctuating velocity	m	=	maximum

Introduction

Examples of upwash jet flow arising from the interaction of opposing plane jets can be found in high lift aerodynamics and other industrial flows for intense turbulence mixing. Besides these practical applications, the interaction of two turbulent jets is also an important flow of academic interest. Among many flows related to multiple jet interactions, the present work focuses on the computation of an upwash jet arising from the two opposing plane wall jets. The flow configuration is schematically shown in Figure 1. The flow has been studied experimentally by several investigators (Gilbert, 1988; Kind and Suthanthiran, 1973; Saripalli, 1985). A very similar flow concerning the interaction of the two opposing curved wall jets has also been studied intensively (Rew and Park, 1988; Park and Rew, 1991). The merged free jet issuing out of the complex interaction zone is known to have similar characteristics with the single, plane turbulent jet. For example, the non-dimensionalized velocity profiles in the self-preserving region are the same for the two flows. Major differences between the two flows, however, lie in the spreading rate and the velocity decay characteristic. It was observed experimentally that the spreading rate of the upwash jet was very much greater than the single, turbulent plane jet. Two colliding plane wall jets produced an upwash jet having the spreading rate of about 0.2 (Gilbert, 1988), while the

International Journal for Numerical Methods for Heat & Fluid Flow
Vol. 8 No. 1, 1998, pp. 64–82.

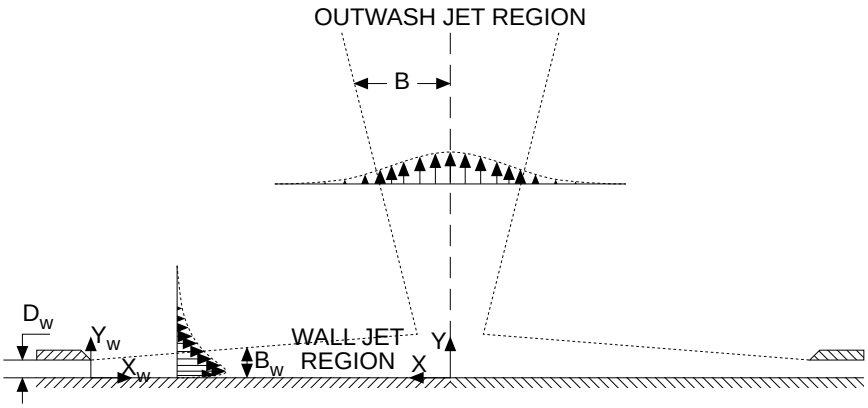

Figure 1.
Upwash jet flow

spreading rate of an ordinary plane jet is about 0.09. Two opposing curved wall jets were reported to produce the outwash jet having the spreading rate of 0.15 (Park and Rew, 1991). It was supposed that the high spreading rate was caused either by intense turbulent diffusion due to very high turbulence level resulting from the collision of the two opposing jets or by unsteady oscillatory behavior of the flow. As shown by Haung and MacInnes (1988) and will be shown in this work, the steady computation utilizing various turbulence models fails to predict the large spreading rate. This suggests that the large spreading rate of the upwash jet is associated with a quasi-periodic unsteadiness of the flow. Evidence to support the unsteady feature of the upwash jet is given in Figure 2. Since the time series of velocity fluctuations for the present flow configuration is not available, we present here the data for the case of the two opposing curved wall jet interaction. Figure 2 illustrates the power spectrum of the axial velocity fluctuation taken at a downstream position (roughly 15 times the wall jet slot height from the cylindrical surface and about 0.4 times the jet half width from the jet centerline) of the outwash jet arising from two symmetric curved wall jets investigated experimentally in our previous works (Rew and Park, 1988; Park and Rew, 1991). We realize that the low frequency oscillations are evidently present in this flow. It is believed that the unsteady nature of the upwash jet from the two plane wall jets should be qualitatively similar to the upwash jet from the two curved wall jets depicted in Figure 2, inferring a similar flow configuration.

As mentioned briefly, the present work discusses the computation of an upwash jet ensuing from two opposing plane wall jets and is an extended study of our earlier presentation (Cho and Park, 1995). The target flow is the one studied experimentally by Gilbert (1988). For the steady computation, the flow field was obtained by integrating the steady version of the Reynolds averaged Navier-Stokes equations employing various turbulence closures. We chose the various k-ε eddy viscosity models and the Reynolds stress transport model. When the Reynolds stress transport model was adopted, several different diffusion term models were tried to investigate the effect of the diffusion term on

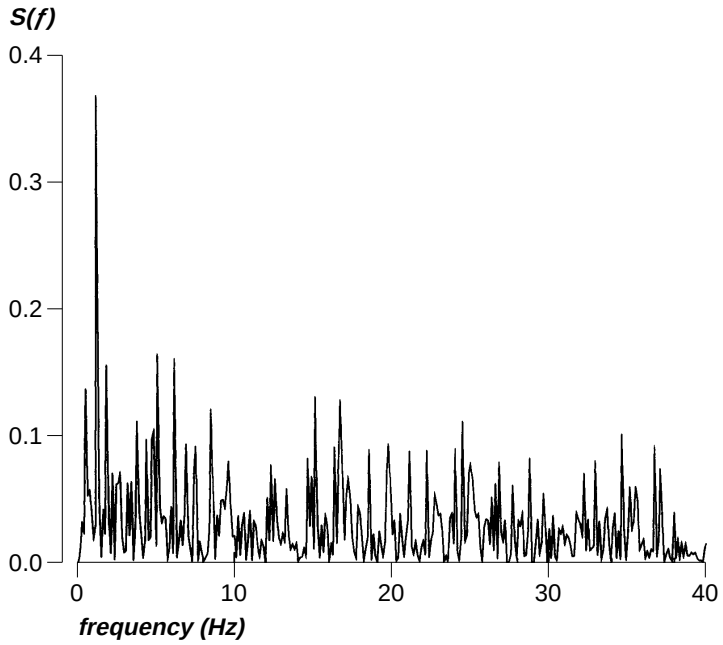

Figure 2.
Power spectrum of axial velocity fluctuation

the flow prediction. The steady flow was computed by enforcing the symmetry condition at the geometric symmetry plane.

In the unsteady computation, an oscillatory behavior of the merged upwash jet was assumed and hence the unsteady solution to account for the oscillatory behavior was sought. An unsteady version of the standard *k-e* eddy viscosity model was used. The computation was performed for the full domain without imposing the symmetry condition to account for the unsteady behavior.

Numerical details

Governing equations and numerical method

We consider the flow to be two-dimensional, incompressible and turbulent. The governing equations are:

$$\frac{\partial U_i}{\partial x_i} = 0 \tag{1}$$

$$\frac{\partial U_i}{\partial t} + \frac{\partial}{\partial x_j}\left(U_j U_i\right) = -\frac{1}{\rho}\frac{\partial P}{\partial x_i} + \frac{\partial}{\partial x_j}\left[\nu\left(\frac{\partial U_i}{\partial x_j} + \frac{\partial U_j}{\partial x_i}\right) - \overline{u_i u_j}\right] \tag{2}$$

To integrate the equations above and the turbulent model equations, to be described later, we developed an incompressible Navier-Stokes solver based on the code developed by Chen (1986). The Chen's code (CNS3D) was based on the hybrid scheme and the *k-e* turbulence model. We essentially rewrote the code to accommodate the Reynolds stress transport model, the consistent quick

formulation (Hayase *et al.*, 1992) for the convection term, and the unsteady term. The governing equations were discretized by a finite volume method on a staggered grid system. The consistent quick scheme (Hayase *et al.*, 1992), known to be very robust among various formulations of the quick scheme, was applied for the momentum equations. The turbulent model equations, however, were discretized by the hybrid scheme instead of the quick, because the quick scheme has a tendency to provoke oscillations in regions of steep property variations (Lien and Leschziner, 1994). It is widely accepted that the turbulence model quantities depends strongly on the source term and hence the discretization of the convection term is less critical. The simple-c procedure (Van Doormaal and Raithby, 1984) was adopted for the iteration to get the velocity and pressure. For the unsteady term, the fully implicit first order discretization in time was employed. The new code was validated against several benchmark flows such as driven cavity flow prior to the present computational work.

Turbulence models

The *k-e* eddy viscosity model, proposed by Launder and Spalding(1974), assumes the following stress-strain relation:

$$-\overline{u_i u_j} = \nu_t\left(\frac{\partial U_i}{\partial x_i} + \frac{\partial U_j}{\partial x_i}\right) - \frac{2}{3}k\delta_{ij} \tag{3}$$

where ν_t is the turbulent eddy viscosity determined from the turbulence energy(k) and its dissipation rate(ε) which obey following transport equations:

$$\frac{\partial}{\partial x_j}\left(U_j k\right) = \frac{\partial}{\partial x_j}\left[\left(\nu + \frac{\nu_t}{\sigma_k}\right)\frac{\partial k}{\partial x_j}\right] + G - \varepsilon \tag{4}$$

$$\frac{\partial}{\partial x_j}\left(U_j \varepsilon\right) = \frac{\partial}{\partial x_j}\left[\left(\nu + \frac{\nu_t}{\sigma_\varepsilon}\right)\frac{\partial \varepsilon}{\partial x_j}\right] + \frac{\varepsilon}{k}\left(C_{\varepsilon 1}G - C_{\varepsilon 2}\varepsilon\right) \tag{5}$$

where, $G = -\overline{u_i u_j}\frac{\partial U_j}{\partial x_j}$ (6)

$$\nu_t = C_\mu \frac{k^2}{\varepsilon} \tag{7}$$

The model constants appearing in the equations above are:

$$C_\mu = 0.09,\ C_{\varepsilon 1} = 1.44,\ C_{\varepsilon 2} = 1.92,\ \sigma_k = 1.0,\ \sigma_\varepsilon = 1.3 \tag{8}$$

We also tested the RNG *k-e* model (Yakhot *et al.*, 1992) and the Bardina's (1988) model to examine the effects of the mean strain rate and mean rotation on the turbulent diffusion. The RNG *k-e* equations are of the same form as the standard *k-e* equations, but assume the different model coefficients evaluated by the renormalization group theory. The RNG *k-e* model by Yakhot *et al.* (1992)

uses the model coefficients which vary with the ratio of the turbulent to the mean strain time scale, η, as described below:

$$C_\mu = 0.085,\ C_{\varepsilon 1} = 1.42,\ C_{\varepsilon 2} = 1.68 + \frac{C_\mu \eta^3 (1 - \eta/4.38)}{1 + 0.012\eta^3},\ \sigma_k = \sigma_\varepsilon = 0.7179 \quad (9)$$

where,

$$\eta = \frac{kS}{\varepsilon},\ S = \left(2S_{ij}S_{ij}\right)^{1/2},\ S_{ij} = \frac{1}{2}\left(\frac{\partial U_i}{\partial x_j} + \frac{\partial U_j}{\partial x_i}\right) \quad (10)$$

Bardina (1988) modified the ε equation in order to account for the effects of mean rotation on the production and removal of the turbulent energy dissipation rate. Bardina's model is represented by the following model coefficients:

$$C_{\varepsilon 1} = 1.50 - 0.015\gamma,\ C_{\varepsilon 2} = \frac{11}{6} + 0.15\gamma \quad (11)$$

where

$$\gamma = \frac{k\Omega}{\varepsilon},\ \Omega = \left(2\Omega_{ij}\Omega_{ij}\right)^{1/2},\ \Omega_{ij} = \frac{1}{2}\left(\frac{\partial U_i}{\partial x_j} - \frac{\partial U_j}{\partial x_i}\right) \quad (12)$$

The Reynolds stress transport model consists of a closed set of transport equations for the Reynolds stress $\overline{u_i u_j}$. The model equations may be written symbolically as,

$$\frac{\partial}{\partial x_j}\left(U_i \overline{u_i u_j}\right) = D_{ij} + G_{ij} + \Phi_{ij} + \varepsilon_{ij} \quad (13)$$

G_{ij}, D_{ij}, Φ_{ij}, ε_{ij} are, respectively, the generation, the diffusion, the pressure-strain correlation, and the dissipation term. We adopted the pressure-strain model suggested by Speziale *et al.* (1991) and Sarkar and Speziale (1990). The return-to-isotropy term ($\Phi_{ij,1}$) and the rapid pressure-strain term ($\Phi_{ij,2}$) given as below comprise the pressure-strain model.

$$\Phi_{ij} = \Phi_{ij,1} + \Phi_{ij,2} \quad (14)$$

$$\Phi_{ij,1} = -\varepsilon\left\{C_1 b_{ij} - 3\left(C_1 - 2\right)\left(b_{ij}^{\ 2} - \frac{1}{3}b_{kk}\delta_{ij}\right)\right\} \quad (15)$$

$$\Phi_{ij,2} = \left(0.8 - C_3^{**}\right)kS_{ij} - C_1^{*}Gb_{ij} + C_4 k\left(b_{ik}S_{jk} + b_{jk}S_{ik} - \frac{2}{3}\delta_{ij}b_{kl}S_{kl}\right) + C_5 k\left(b_{ik}\Omega_{jk} + b_{jk}\Omega_{ik}\right) \quad (16)$$

where,

$$b_{ij} = \frac{\overline{u_i u_j}}{2k} - \frac{1}{3}\delta_{ij},$$

$$C_3^{**} = C_3^{*}\left(b_{ij}b_{ij}\right)^{1/2},\ C_1 = 3.4,\ C_1^{*} = 1.8,\ C_3^{*} = 1.3,\ C_4 = 1.25,\ C_5 = 0.4 \tag{17}$$

S_{ij} and Ω_{ij} are the same as given in equations (11) and (12).

The three diffusion models proposed respectively by Daly and Harlow (1970) (DH), Hanjalic and Launder (1972) (HL) and Mellor and Herring (1973) (MH) were selected to scrutinize the effect of the diffusion term on the spreading rate. These models are given respectively as:

$$\text{DH: } D_{ij} = \frac{\partial}{\partial x_k}\left\{C_{s1}\frac{k}{\varepsilon}\left[\overline{u_k u_l}\frac{\partial \overline{u_i u_j}}{\partial x_l}\right]\right\} \tag{18}$$

$$\text{HL: } D_{ij} = \frac{\partial}{\partial x_k}\left\{C_{s2}\frac{k}{\varepsilon}\left[\overline{u_i u_l}\frac{\partial \overline{u_j u_k}}{\partial x_l} + \overline{u_j u_l}\frac{\partial \overline{u_i u_k}}{\partial x_l} + \overline{u_k u_l}\frac{\partial \overline{u_i u_j}}{\partial x_l}\right]\right\} \tag{19}$$

$$\text{MH: } D_{ij} = \frac{\partial}{\partial x_k}\left\{C_{s3}\frac{k^2}{\varepsilon}\left[\frac{\partial \overline{u_i u_j}}{\partial x_k} + \frac{\partial \overline{u_j u_k}}{\partial x_j} + \frac{\partial \overline{u_j u_k}}{\partial x_i}\right]\right\} \tag{20}$$

$$\text{where, } C_{s1} = 0.22, C_{s2} = 0.22, C_{s3} = \frac{0.22}{3}$$

These models are essentially gradient diffusion models focusing mainly on the turbulent diffusion due to the triple moments of velocity fluctuations. To model the pressure diffusion additionally by large scale turbulence, Kim and Chung (1994) (KC) proposed the following pressure-velocity diffusion model based on the concept of convection velocity, which we add to the HL model:

$$\text{KC: } -\frac{\overline{pu_i}}{\rho} = C_p C_{c1} f_c \frac{\overline{u_i u_n u_n}}{\varepsilon}\frac{\partial U_j}{\partial x_l}\overline{u_i u_j} + \frac{1}{2}C_p \overline{u_i u_j u_j} \tag{21}$$

where

$$f_c = \exp(-C_{c2}/),\ / = \left(k/U_m U_m\right)^{1/2},\ C_{c1} = 0.7,\ C_{c2} = 0.8,\ C_p = 0.2 \tag{22}$$

For the ε equation, we selected the model of Launder *et al.* (1975). The diffusion term in the ε equation was remodeled in the following form to explicitly include the Reynolds stress:

$$\varepsilon_{ij} = -\frac{2}{3}\varepsilon\delta_{ij} \tag{23}$$

$$\frac{\partial}{\partial x_j}\left(U_j\varepsilon\right) = C_\varepsilon \frac{k}{\varepsilon}\frac{\partial}{\partial x_k}\left[\overline{u_k u_m}\frac{\partial \varepsilon}{\partial x_m}\right] + \frac{\varepsilon}{k}\left(C_{\varepsilon 1}G - C_{\varepsilon 2}\varepsilon\right) \tag{24}$$

$$\text{where, } C_\varepsilon = 0.18 \tag{25}$$

Boundary conditions and convergence criteria

As shown in Figure 1, the jet nozzle height (D_w) was 1cm and the nozzle to nozzle distance was 84cm. The jet exit velocity was set to 67m/s. The Reynolds number based on the jet exit velocity and jet nozzle height was 4.68×10^4.

The steady upwash jet flow can be computed by enforcing the symmetry condition at the geometric symmetry plane. This halves the computational domain as shown in Figure 3. Inlet velocity profile was specified to be uniform and the inlet turbulence energy k was given from the experimental values (Gilbert, 1988). Along the entrainment and the outflow boundaries, constant static pressure was assumed and the gradient of tangential velocity was set to be zero. The velocity normal to the boundary was then calculated from the continuity equation. Zhu (1992) and Laschefski *et al.* (1994) adopted these boundary conditions in their computations of the impinging jet flow and the radial jet reattachment flow respectively. The wall function method was employed on the base surface to impose the wall boundary condition. The boundary value of the Reynolds stress was obtained from the wall shear stress as given in Launder *et al.* (1975) The use of wall function, when the solution obtained by using the wall function and the one with the near wall low Reynolds number model were compared, was found not to influence the upwash jet flow.

The unsteady computation for an oscillatory upwash jet was performed for the full domain without imposing symmetry condition. While the wall and the entrainment boundary conditions were specified the same as in the steady computation, the outflow boundary condition was specified as given below.

$$\frac{\partial \phi}{\partial t} + C\frac{\partial \phi}{\partial n} = 0 \qquad (26)$$

where ϕ=U, V, k, ε

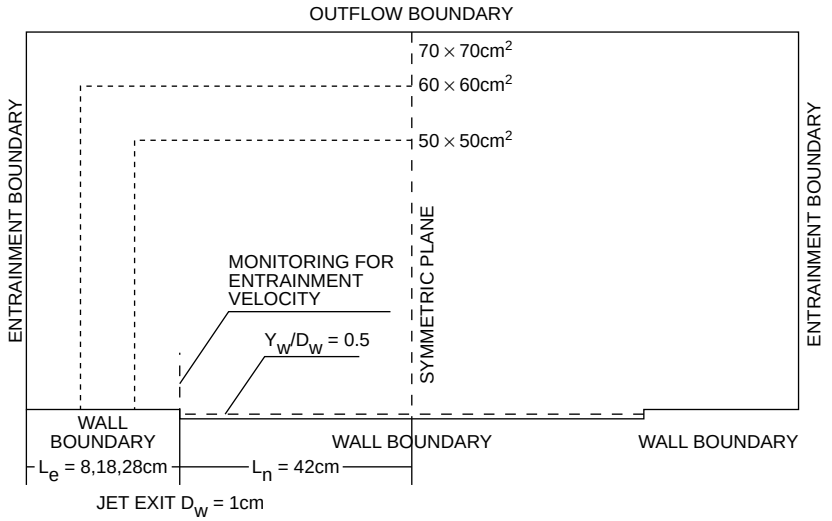

Figure 3.
Computational domain

C is the representative convection velocity at the outflow boundary and n is the normal co-ordinate to the boundary. Physically equation (26) implies the convection of frozen vector field with a convection velocity C. The boundary condition, often called the Sommerfeld radiation condition, was first proposed by Orlanski (1976) mainly for hyperbolic flows, and was applied to various incompressible flows (Kobayashi *et al.*, 1994; Pauley, 1994). It was pointed out by Sani and Gresho (1994) that the quality of result was somewhat dependent on the choice of C in the transient problem, and the average normal velocity through the outflow boundary is a reasonable candidate for C for the duct flow and the boundary layer flow. Because the present computational domain is not confined with end walls, it is ambiguous to specify the convection velocity C as the average normal velocity. After several trials, we found that evaluation of C by the extrapolation from the interior node values is an adequate choice.

The steady solution was assumed to be converged when the sum of the dimensionless residuals of the velocity and the pressure was less than 1×10^{-5}. In the case of the unsteady computation, the dimensionless time step, $\frac{\Delta t}{D_w/U_j}$, of 200 was used. At each time step, the same convergence criteria as in the steady case were imposed. One period of the jet oscillation was approximately equal to the time interval of about 26 time steps. The use of smaller time step than 200 did not alter the results of the unsteady computation. However, when we tried more than twice larger time steps than 200, the oscillatory pattern of velocity profiles became distorted.

Results and disussions

Steady case

Determination of the computational domain is a non-trivial issue when the physical flow domain is unbounded. To decide an adequate size of the computational domain, we carried out preliminary computations for various domain sizes. Figure 4 compares the entrainment velocity profile variations along the vertical line off the jet exit, depending on the size of the computational domain. Gilbert (1988) found that the entrainment velocity was 0.097 times the mean exit velocity. As seen in Figure 4, we found that the $70 \times 70 \text{cm}^2$ computational domain should be satisfactory. A simple rectangular grid system with appropriate stretching was used in this computation. The grid system was clustered in the regions of wall jet and outwash jet, the smallest grid size being 0.1×0.48 cm^2. To examine the grid dependency of the solution, computations were performed on four different grid systems (107×121, 94×109, 83×92, 66×77). A result of this test is illustrated in Figure 5, which demonstrates that the 94×109 grid is sufficient for the present computation. The grid dependency and the computational domain size tests were carried out using the k-ε model.

The accuracy of prediction in the upwash region is expected to be affected by the predicted behavior of the wall jet development and collision. As pointed out by Haung and MacInnes (1988), the wall jet growth rates predicted by the various turbulence models were in good agreement with experimental data.

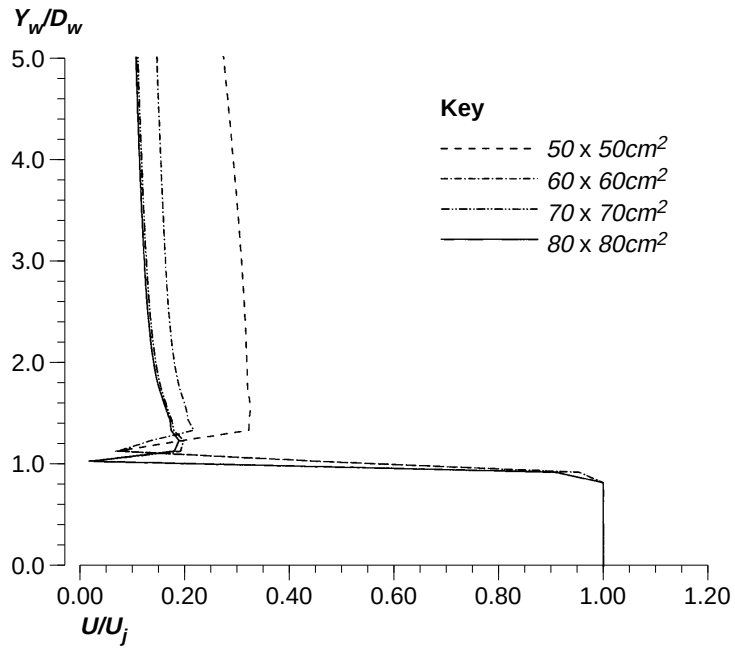

Figure 4.
Entrainment velocity variations with computational domain size

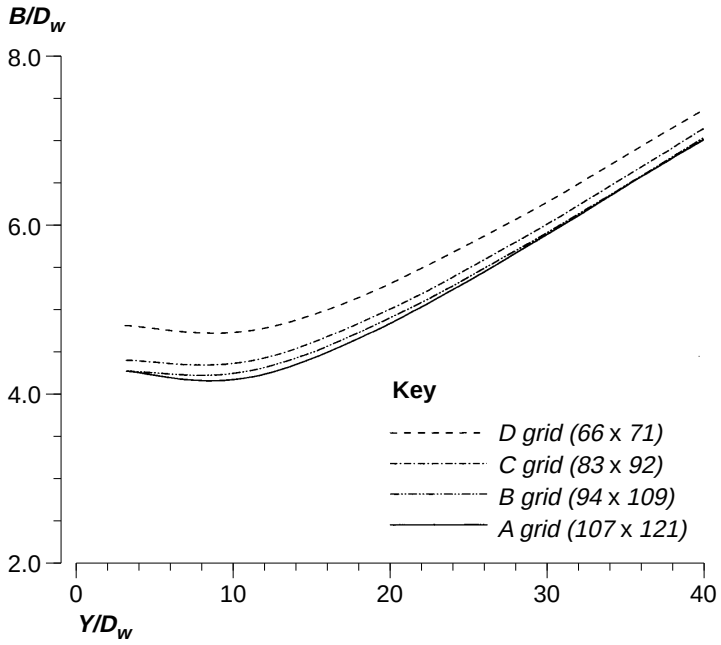

Figure 5.
Jet half-width distribution for various grid densities

Figure 6 compares the axial velocity parallel to the wall, U_w, at the fixed height of $Y_w/D_w = 0.5$ line. It is clearly seen that the velocity profile computed with the Reynolds stress model is in much better agreement with the Gilbert's experimental data. Because of the enforced symmetry condition, U_w velocity predicted at the symmetric plane is zero. We note, however, that the experimental value is somewhat different from zero at the line of symmetry. The experimental value is read to be about 0.2 times the mean exit velocity. The non-zero mean velocity at the line of symmetry was perhaps caused either by a slight asymmetry of the experimental setup or by the ambiguity of the hot-wire measurement at very low velocity. As will be shown later, minor discrepancies among the velocity profiles both in the wall jet and in the upwash jet region caused by the different choice of the turbulence models are not essentially related to the spreading rate of the upwash jet.

To examine the effect of turbulence models on the spreading rate of the upwash jet, we tried three different two-equation turbulence models: the standard k-ε model, the RNG k-ε model, and the Bardina's model. Figures 7 and 8 show, respectively, the jet centerline velocity decay, represented by the distribution of the maximum axial velocity V_m and the jet half width (B) growth characteristics. It is seen that the jet centerline velocity profiles is overpredicted and the jet half width is underpredicted significantly. All of these three models exhibit similar behavior. The results depicted in these figures clearly indicate that the minor model variations in the two-equation level can not account for the large spreading rate of the upwash jet. Although the spreading rate and hence

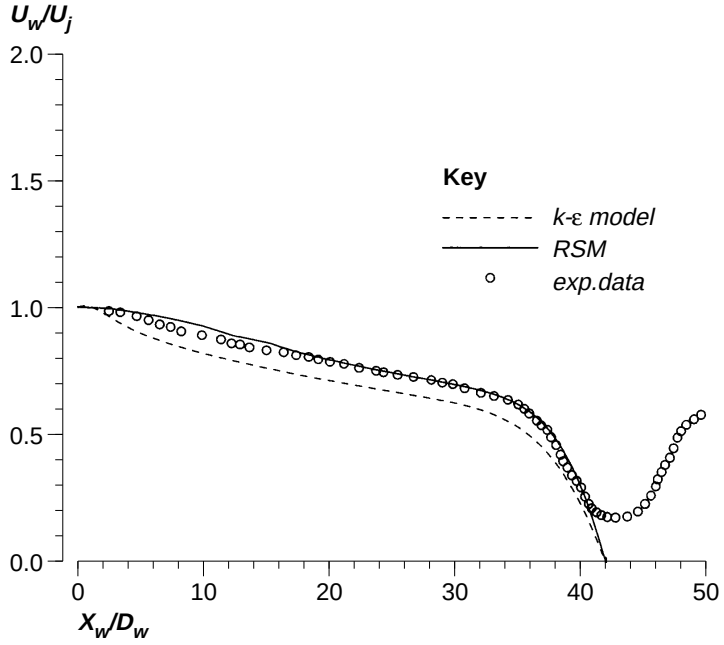

Figure 6.
Mean velocity distribution along $Y_w/D_w = 0.5$ line

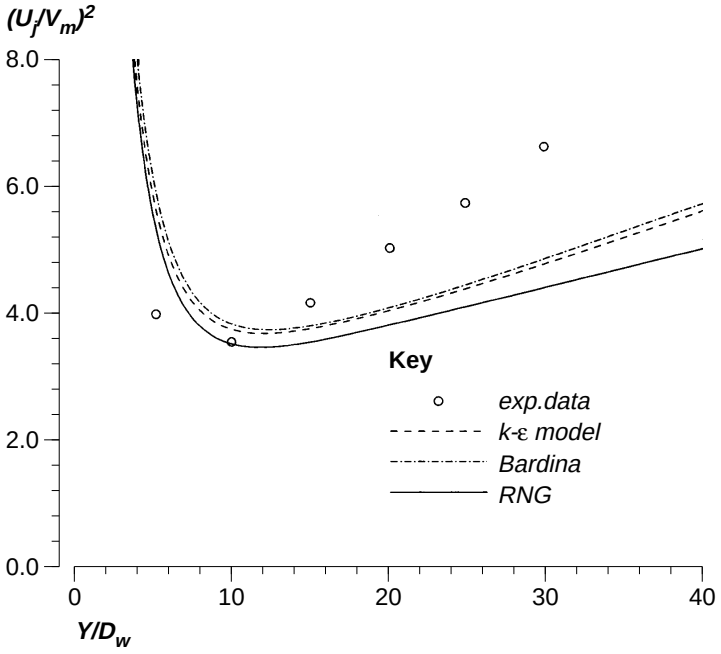

Figure 7.
Velocity decay curve of the upwash jet (k-ε model; V_m = jet centerline velocity; U_j = jet exit velocity at the nozzle)

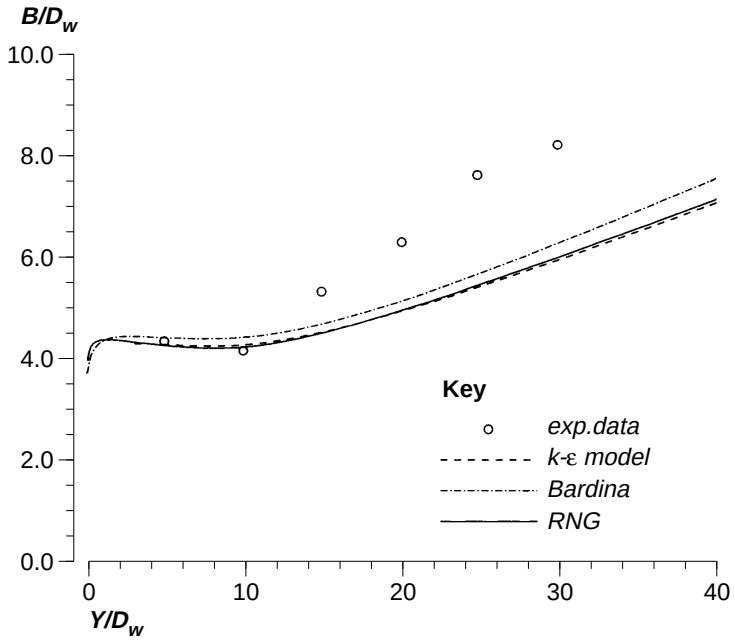

Figure 8.
Jet half-width distribution of the upwash jet (k-ε model)

the velocity decay characteristic evaluated from computational results are far from being agreeable to the experimental data, the dimensionless velocity profiles, if non-dimensionalized as is normally done to describe jet flows, are found to be in excellent agreement with the experimental data. Owing to the self preserving nature of the free jet flow, the agreement with the experimental data is expected at a location far downstream where the upwash jet flow development becomes approximately self-preserving. This is illustrated in Figure 9, where the dimensionless profiles at the two downstream locations(Y/D_w = 20, 40) are given. In the figures of the top row, the velocity and the distance are normalized respectively by the jet exit velocity and the nozzle height. The discrepancy between the predictions and the experimental data is clearly noted. However, if the same data are replotted via the normalization with the jet centerline velocity (V_m) and the jet half-width (B), we see an excellent agreement with the experimental data as depicted in the figures of the bottom row. We comment here that the experimental data given in Figure 8 are the data that could only be selected with confidence from the published work of Gilbert (1988), where the data taken at various downstream stations were overlaid. The trends observed in the results discussed above still hold in the computational results obtained using the Reynolds stress transport model.

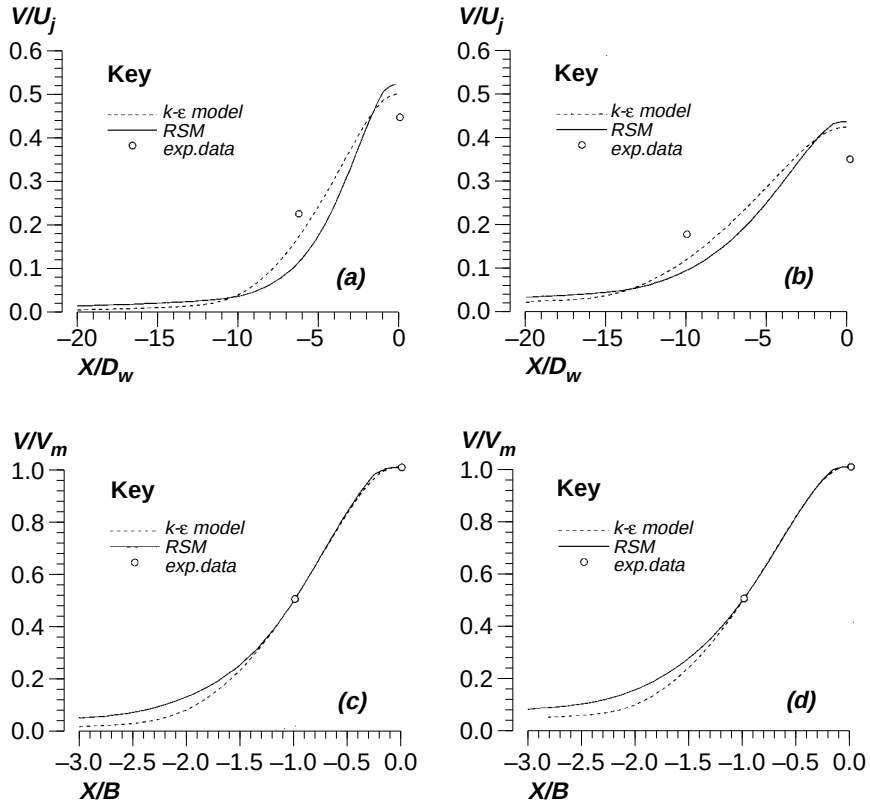

Figure 9. Comparison of dimensionless axial velocity profiles: (a) V/U_j at Y/D_w = 20; (b) V/U_j at Y/D_w = 40; (c) V/V_m at Y/D_w = 20; (d) V/V_m at Y/D_w = 40

Figures 10 and 11 show the computed results using the Reynolds stress models with diffusion term model variations (DH, HL, MH, HL + KC). Although the closure models vary considerably, the results show rather poor agreement with

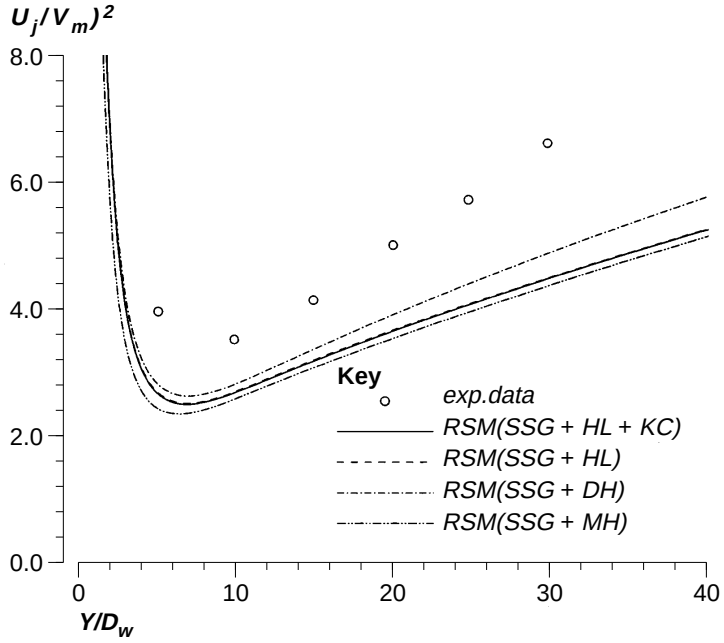

Figure 10.
Velocity decay curve of the upwash jet (Reynolds stress model; V_m = jet centerline velocity; U_j = jet exit velocity at the nozzle)

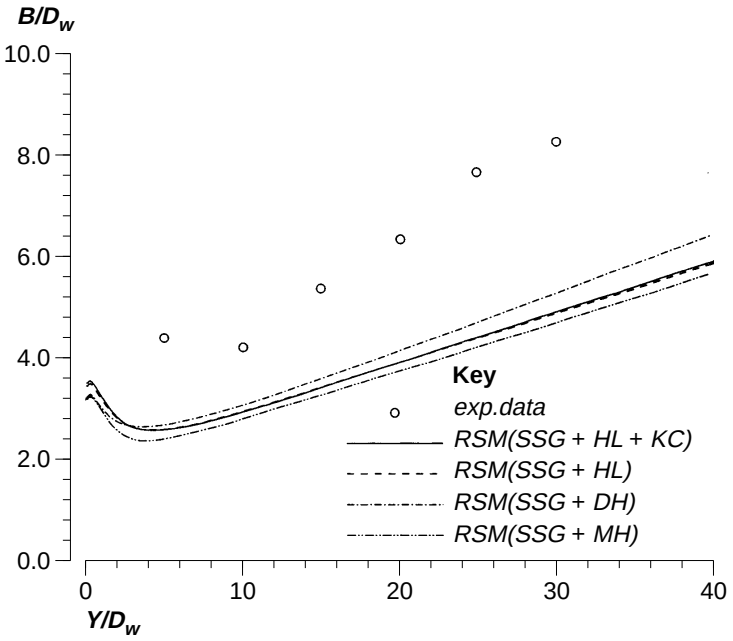

Figure 11.
Jet half-width distributions of the upwash jet (Reynolds stress model)

the experimental data. In the present work, all the turbulence models employed predicted a spreading rate of the upwash jet more or less equal to the ordinary plane jet. Considering the fact that the currently available turbulence models failed to predict successfully the very large spreading rate of the upwash jet, the problem may better be tackled with a new viewpoint other than the turbulence model studies. Obviously, an alternative way is to take the unsteadiness of the flow into account.

Unsteady case

Results from the steady computation led us to believe that the rapid growth rate of the upwash jet must be associated with a large-scale oscillatory behavior of the flow. To be rigorous, such flows should be computed via either large eddy simulation or direct numerical simulation. However, these approaches require enormous computational resources and effort since the calculation should proceed with the full three-dimensional unsteady Navier-Stokes equations and the very dense grid and short time step to resolve the turbulence scales sufficiently. An alternative engineering approach is to adopt the turbulence model equation assuming that the large-scale motion is decoupled with the random turbulent motion of the flow. We adopt this procedure in the present work. Typical turbulent time scale of the present steady jet is of order 0.01sec. On the contrary, the oscillatory time scale is of order 1 sec. Thus, the ratio of the time scales is approximately 100. Hence, we conjecture that the turbulence characteristic is decoupled with the oscillatory behavior. We employ the unsteady version of the standard k-ε model of Kato and Launder (1993) as used in their calculation of the turbulent wake behind a square rod. For the unsteady version, they modified the kinetic energy production term, G, as follows:

$$G = C_\mu \varepsilon S \Omega \tag{27}$$

$$\text{where,} \quad S = \frac{k}{\varepsilon}\sqrt{\frac{1}{2}\left(\frac{\partial U_i}{\partial x_j} + \frac{\partial U_j}{\partial x_i}\right)^2} \quad , \quad \Omega = \frac{k}{\varepsilon}\sqrt{\frac{1}{2}\left(\frac{\partial U_i}{\partial x_j} - \frac{\partial U_j}{\partial x_i}\right)^2} \tag{28}$$

As mentioned previously, the convective boundary condition is employed for the outflow boundary. The converged steady solution is used as the initial data. To examine the dependency of the unsteady behavior of the jet on the outflow boundary position, we tried an $80 \times 80\text{cm}^2$ grid system. We found that the jet oscillation was not essentially influenced. The amplitude of U velocity oscillation (Figure 12) at $Y/D_w = 40$, however, was increased by 2 per cent. We thus concluded that the $70 \times 70\text{cm}^2$ grid system should also be satisfactory for the present unsteady computation.

The U velocity (transverse velocity) at the two locations ($Y/D_w = 20, 40$) on the centerline is shown as a time series in Figure 12. A time scale based on the jet exit velocity and the jet nozzle height can be defined as D_w/U_j, which is 1.4925×10^{-4}sec for the present case. Another time scale based on the two-

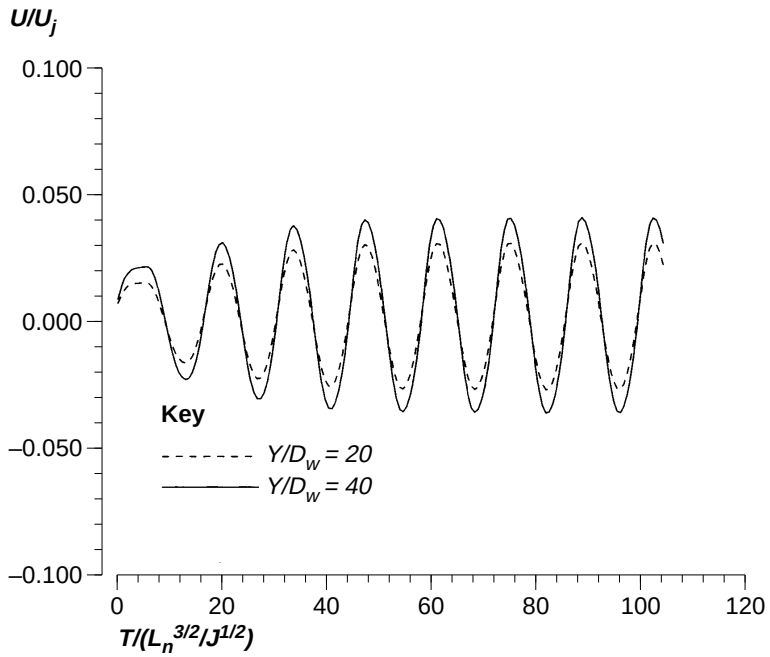

Figure 12.
Time history of transverse velocity at two elevations (Y/D_w = 20, 40) on the centerline

dimensional jet exit momentum flux ($J = D_w U_j^2$) and the half of nozzle to nozzle distance($2L_n$) can also be used, which is $L_n^{3/2}/J^{1/2} = 4.063 \times 10^{-2}$sec. The nondimensional period of oscillation at $Y/D_w = 40$ (see Figure 12) was about 13.67, and the corresponding Strouhal number ($St = f L_n^{3/2}/J^{1/2}$) was 0.073. The period oscillation corresponded to 0.555sec.

The unsteady nature of the V velocity (axial velocity) for one period along the $Y/D_w = 40$ line is shown in Figure 13. We clearly see the periodic swing of almost the same velocity profile in transverse direction. The frequency of oscillation is slightly less than 2 Hz. The oscillation of the jet obviously results in a larger jet width in a time averaged sense. The time-averaged velocity profile for a period at Y/D_w=40 is shown in Figure 14. We clearly see that the jet centerline velocity is decreased and the jet half width is increased, which brings the predicted results closer to the experimental data.

The jet half width distribution obtained by the time averaging of the periodic velocity profile is shown in Figure 15. The spreading rate was estimated to be 0.18, in contrast to the spreading rate of 0.10 for the case of the steady computation. This clearly indicates that the unsteady computation significantly improved the prediction of the upwash jet flow characteristics.

Conclusion

Computation of the upwash jet evolving from two opposing wall jets was performed by using both the steady and the unsteady computational

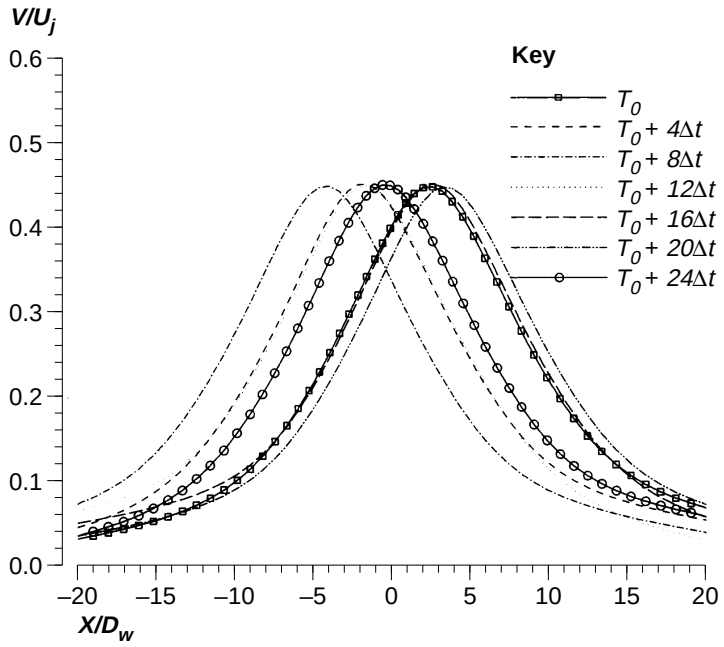

Figure 13. Axial velocity variations at $Y/D_w = 40$ for a period of flow oscillation

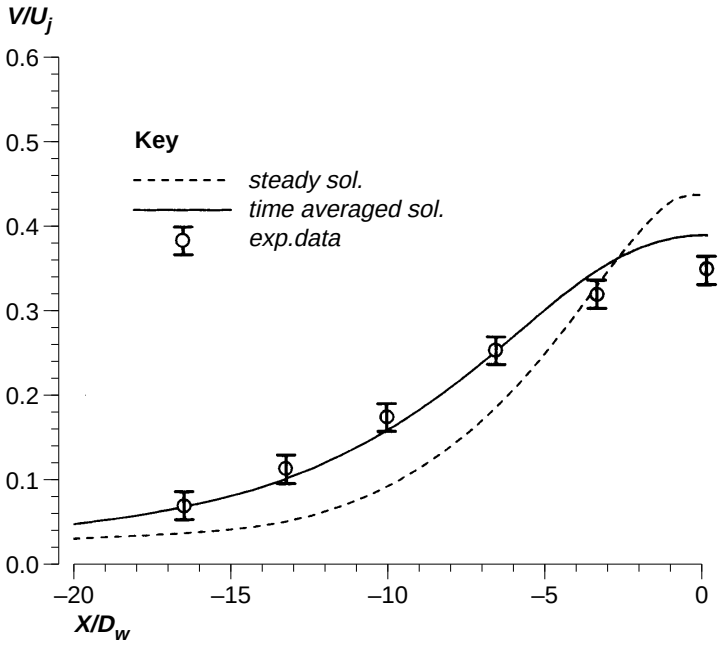

Figure 14. Comparison of axial velocity distributions for the steady and the unsteady computations at $Y/D_w = 40$

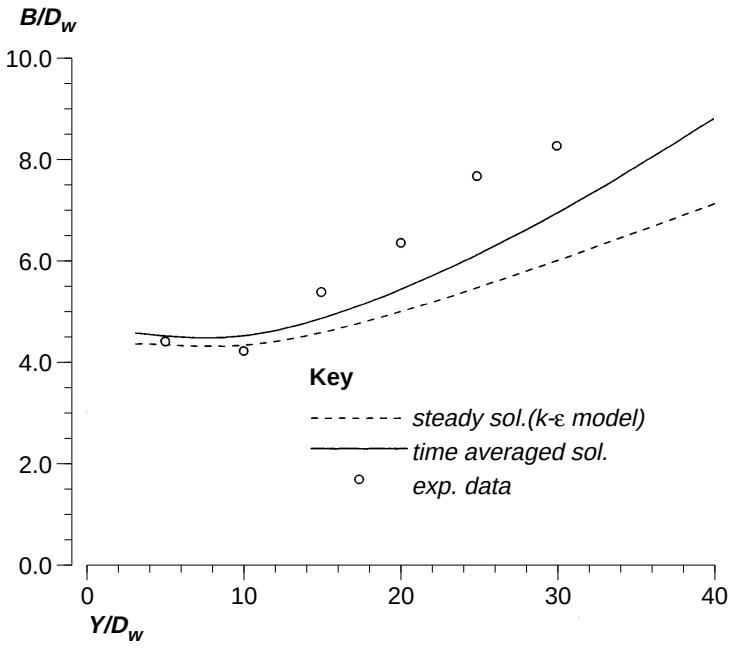

Figure 15.
Jet half-width distributions for the steady and the unsteady computations

approaches. From the steady computational results, we found that all the turbulence models employed in the present work did not predict satisfactorily the flow characteristics of the upwash jet. The unsteady computation with the k-ε model resulted in a periodically oscillating flow. The spreading rate estimated from the time-averaged velocity profile was found to be in much better agreement with the experimental data. Comparison of the velocity profiles led us to believe that the present approach successfully mimicked the oscillatory behavior of the upwash jet.

References

Bardina, J. (1988), "Turbulence modelling based on direct simulation of the Navier-Stokes equations", *Proceedings of AIAA/ASME/SIAM/APS 1st National Fluid Dynamics Congress*, Cincinnati, OH, 25-28 July, pp. 539-46.

Chen, Y.S. (1986), "A computer code for three-dimensional incompressible flows using non orthogonal body-fitted coordinate systems", NASA CR-178818.

Cho, S.H. and Park, S.O. (1995), "Computation of an outwash jet flow arising from two opposing plane wall jets", *Proceedings of Ninth Int. Conf. Numerical Methods in Laminar and Turbulent Flow*, Atlanta, GA, 10-14 July, pp. 1019-30.

Daly, B.J. and Harlow, F.H. (1970), "Transport equation of turbulence", *Phys. Fluids*, Vol. 13, pp. 2634-49.

Gilbert, B.L. (1988), "Turbulence measurement in a two-dimensional upwash", *AIAA J.*, Vol. 26, pp. 10-14.

Hanjalic, K. and Launder, B.E. (1972), "A Reynolds stress model of turbulence and its application to thin shear flows", *J. Fluid Mech.*, Vol. 52, pp. 609-38.

Haung, P.G. and MacInnes, J.M. (1988), "Modelling the outwash flow arising from two colliding turbulent jets", *Proceedings of AIAA/ASME/SIAM/APS 1st National Fluid Dynamics Congress*, Cincinnati, OH, 25-28 July, pp. 955-64.

Hayase, T., Humprey, J.A.C. and Grief, R. (1992), "A consistently formulated QUICK scheme for fast and stable convergence using finite-volume iterative calculation procedures", *J. Comp. Phys.*, Vol. 98, pp. 108-18.

Kato, M. and Launder, B.E. (1993), "The modelling of turbulent flow around stationary and vibrating square cylinders", *Proceedings of Ninth Symp. Turbulent Shear Flow*, Kyoto, 16-18 August, pp. 10-14.

Kim, S.G. and Chung, M.K. (1994), "Spatial transport of Reynolds stress by pressure fluctuations", *Phys. Fluids*, Vol. 6, pp. 3507-09.

Kind, R.J. and Suthanthiran, K. (1973), "The interaction of two opposing plane turbulent wall jets", *J. Fluid Mech.*, Vol. 58, pp. 389-402.

Kobayashi, M.M., Pereira, J.C.F. and Sousa, J.M.M. (1994), "Comparison of several open boundary numerical treatments for the recirculating flows", *Int. J. Numer. Meth. Fluids.*, Vol. 16, pp. 403-19.

Laschefski, H., Braess, D., Haneke, H. and Mitra, N.K. (1994), "Numerical investigations of radial jet reattachment flows", *Int. J. Numer. Meth. Eng.*, Vol. 18, pp. 629-46.

Launder, B.E. and Spalding, D.B. (1974), "The numerical computation of turbulent flows", *Comp. Meth. Appl. Mech. Eng.*, Vol. 3, pp. 269-89.

Launder, B.E., Reece, G.J. and Rodi, W. (1975), "Progress in the development of a Reynolds stress turbulence closure", *J. Fluid Mech.*, Vol. 68, pp. 537-66

Lien, F.S. and Leschziner, M.A. (1994), "A general non-orthogonal collocated finite volume algorithm for turbulent flow at all speeds incorporating second-moment turbulence-transport closure, Part 1: Computational implementation", *Comp. Meth. Appl. Mech. Eng.*, Vol. 114, pp. 123-48.

Mellor, G.L. and Herring, H.J. (1973), "A survey of mean turbulent field closure", *AIAA J.*, Vol. 11, pp. 590-9.

Orlanski, I. (1976), "A simple boundary condition for unbounded hyperbolic flows", *J. Comp. Phys.*, Vol. 21, pp. 251-69.

Park, S.O. and Rew, H.S. (1991), "Turbulence measurement in a merged jet from two opposing curved wall jets", *Exp. Fluids*, Vol. 10, pp. 241-50.

Pauley, L.L. (1994), "Structure of local pressure-driven three dimensional transient boundary layer separation", *AIAA J.*, Vol. 32, pp. 997-1005.

Rew, H.S. and Park, S.O. (1988), "The interaction of two opposing asymmetric curved wall jets", *Exp. Fluids*, Vol. 6, pp. 243-52.

Sani, R.L. and Gresho, P.M. (1994), "Resume and remarks on the open boundary condition minisymposium", *Int. J. Numer. Meth. Eng.*, Vol. 18, pp. 983-1008.

Saripalli, K.R. (1985), "Laser doppler velocimeter measurements in 3D impinging twin jet fountain flows", *AIAA paper No.* 85, p. 4036.

Sarkar, S. and Speziale, C.G. (1990), "A simple nonlinear model for the return to isotropy in turbulence", *Phys. Fluids*, Vol. A2, pp. 84-93.

Speziale, C.G., Sarkar, S. and Gatski, T.B. (1991), "Modelling of the pressure-strain correlation of turbulence: an invariant dynamical system approach", *J. Fluid Mech.*, Vol. 227, pp. 245-72.

Van Doormaal, J.P. and Raithby, G.D. (1984), "Enhancement of the SIMPLE method for predicting incompressible fluid flow", *Numer. Heat Transfer*, Vol. 7, pp. 147-63.

Yakhot, V., Orszag, S.A., Thangam, S., Gatski, T.B. and Speziale, C.G. (1992), "Development of turbulence models for shear flows by a double expansion technique", *Phys. Fluids*, Vol. A4, pp. 1510-20

Zhu, J. (1992), "On the higher-order bounded discretization schemes for finite volume computations of incompressible flows", *Comp. Meth. Appl. Mech. Eng.*, Vol. 98, pp. 345-60.